X-661-76-221

PREPRINT

TMX 71198

USE OF THIN IONIZATION CALORIMETERS FOR MEASUREMENTS OF COSMIC RAY ENERGY SPECTRA

W. V. JONES
J. S. ORMES
W. K. H. SCHMIDT

SEPTEMBER 1976

GSFC — GODDARD SPACE FLIGHT CENTER
GREENBELT, MARYLAND

USE OF THIN IONIZATION CALORIMETERS FOR MEASUREMENTS OF COSMIC RAY ENERGY SPECTRA

W. Vernon Jones*, Jonathan F. Ormes, and Wolfgang K. H. Schmidt**
National Aeronautics and Space Administration
Goddard Space Flight Center
Laboratory for High Energy Astrophysics
Cosmic Radiations Branch
Greenbelt, Maryland 20771

*On Sabbatical from Louisiana State University, Baton Rouge, LA
**NAS/NRC Resident Research Associate

Abstract

The reliability of performing measurements of cosmic ray energy spectra with a thin ionization calorimeter has been investigated. Two Monte Carlo simulations were used to determine whether energy response fluctuations would cause measured spectra to be different from the primary spectra. First, Gaussian distributions were assumed for the calorimeter energy resolutions which (a) did not change with energy, (b) increased with energy, and (c) decreased with energy. The second method employed a detailed Monte Carlo simulation of cascades from an isotropic flux of protons, with incident energies representing (a) a simple power law, (b) a power law with a bend, and (c) an energy dependent spectral exponent. The results show that as long as the energy resolution does not change significantly with energy, the spectral indices can be reliably determined even for $\sigma_E/E = 50\%$. However, if the energy resolution is strongly energy dependent, the measured spectra do not reproduce the true spectra. Energy resolutions greatly improving with energy result in measured spectra that are too steep, while resolutions getting much worse with energy cause the measured spectra to be too flat. Since thin calorimeters have energy resolution approximately constant with energy, they offer a viable means for measuring power law spectra. They are also suitable for detecting spectral bends or energy dependent spectral exponents, provided sufficient exposure is available.

1. Introduction

The energy distributions of cosmic rays carry information about the acceleration processes, about the sources of the particles, and about their propagation through and interaction with the interstellar medium.

As such they contain important astrophysical information about the origin and life history of these particles.

Existing data[1-8] on primary cosmic rays indicate that they typically have energy spectra of the form

$$\frac{dN}{dE} = K\, E^{-\gamma} \tag{1}$$

Different particle species are represented by different values of K and γ. For example, protons have a spectral index $\gamma \simeq 2.7$ while iron nuclei may have a spectral index as low as $\gamma \simeq 2.1$. Examples of recent spectral measurements for protons and helium are shown in Fig. 1a, and for other nuclei in Fig. 1b. We know from previous experiments that for all species there is a rapid decrease in intensity with energy. Consequently, the major problem in designing instruments for high energy spectral measurements is how to achieve the maximum collecting area with a detector which has energy resolution sufficient for a reliable measurement of a power law primary spectrum. In addition, measurements should be capable of reflecting a spectrum which has different indices in different energy ranges; i.e.,

$$\begin{aligned} \frac{dN}{dE} &= K_1\, E^{-\gamma_1}, \quad E_o < E \leq E_1 \\ &= K_2\, E^{-\gamma_2}, \quad E_1 < E \leq E_2. \end{aligned} \tag{2}$$

Such a knee in the proton spectrum has been reported by Grigorov to occur just above 1000 GeV.[9]

It also may be that $\gamma = \gamma(E)$ in some energy range, in which case the simple power law interpretation is invalid. We do not expect sharply structured features, particularly monoenergetic lines, in the energy spectra of charged particles, even though they may be present at the

source. The stochastic scattering due to the propagation processes would spread the energies and at the same time cause the arrival directions to be distributed isotropically. Furthermore, we do not expect narrow-band time structure such as the pulsations observed in radio, optical, and X-ray observations. The interstellar magnetic fields would spread the arrival times at earth of a synchronous pulse of charged particles emitted with small directional dispersion at the source.

To reiterate, we expect to measure relatively smooth spectra, in both energy and time, for each particle species, and we expect the energy spectra to be generally of the form given in Eq. 1. However we must be able to detect two or more spectral indices in different energy ranges as indicated by Eq. 2 or even be able to detect an energy dependent spectral exponent.

It is our objective here to show that a thin ionization calorimeter will suffice to measure the cosmic ray spectra in either of these cases, provided ample exposure time is available to cover the requisite energy range for distinguishing among them. Since an ionization calorimeter can measure primary energies over an essentially unlimited energy range, it is perhaps the only device which can accomplish this task in a single experiment. Most other energy measurement techniques are valid over limited energy ranges. Therefore, their use would require either several experiments operating in different ranges or several techniques valid for different ranges in a single experiment. An "ionization calorimeter" basically consists of an amount of matter where high energy particles suffer successive interactions thereby building up a shower or cascade

of particles. This way the particles transfer a significant fraction of their original kinetic energy to ionization of the material which can be measured. Thus the energy of the primary particle is determined by a method reminiscent of calorimetric measurements.

Essentially, a thin calorimeter measures the energy transferred to electron-photon cascades in the first interaction of the primary particle. The energy resolution, therefore, depends on the fluctuations in the amount of energy going into the production of neutral pions. The energy resolution improves as the calorimeter is made deeper because additional interactions occur. The additional interactions result in a larger portion of the incident energy appearing in the electromagnetic component so that at larger fraction of the incident energy is measured and thus fluctuations are decreased.

Detailed investigations using accelerator calibration, and Monte Carlo calculations bave been carried out on the energy response of ionization calorimeters to monoenergetic particles.[10-23] From that work we have a reasonable understanding of how the energy resolution changes with calorimeter depths, different absorber materials, different particle species, and different primary energies. A brief recapitulation of some pertinent results is given in Sec. 2. However, in this paper we primarily address the problem of how the energy resolution affects the spectral indices to be measured.

We present in Sec. 3 some simple analytical arguments related to the problem. Essentially the same results were given in Ref. 8. They are repeated here for completeness and for setting the framework of the subsequent Monte Carlo results using several different energy resolution distributions. In Sec. 4. we present results of a Monte Carlo study

using Gaussian distributions for the energy resolutions. The distributions were characterized by the standard deviations σ/μ, where μ is the mean of the distribution. We hereafter abbreviate σ/μ as σ. Calculations were carried out for cases (a) where σ remained constant with energy, (b) where σ increased with energy, and (c) where σ decreased with energy. In Sec. 5. we describe results of a more direct simulation of an experiment; i.e., Monte Carlo-calculations were carried out for an isotropic flux of protons incident on a thin calorimeter whose energies were selected from input energy spectra. Results are presented (a) for a simple power law, (b) for a power law with a bend, and (c) for an energy dependent spectral exponent. In this latter method no specific assumptions were made about how the energy resolution changes with energy. The resolution for each energy was that predicted y- the Monte-Carlo model used to calculate the cascades. As pointed out in Ref. 23 the model is in good agreement with both accelerator and cosmic ray measurements of the cascade development. Consequently, the results given in Sec. 5. should predict the situation encountered in an experiment reasonably well.

2. Energy Resolution of Calorimeters

Investigations of the response of an ionization calorimeter to monoenergetic particles have shown that when a high energy hadron enters a large, dense absorber, almost all of the hadron's primary energy E_o is dissipated via ionization and excitation of the absorbing material. The area under the curve of ionization energy versus depth in the absorber provides a measure of E_o. For a very deep absorber the energy deposited can be represented by Gaussian distributions whose widths decrease as the beam energy increases.[17-21] An infinitely deep calorimeter will provide

energy resolution limited only by the statistical nature of the cascade process itself and by the frequency of sampling of the ionization energy. We will assume throughout this paper that the sampling frequency is sufficient to have a negligible effect on the resolution. The minimum depth which can be used for cosmic ray measurements depends on the energy resolution acceptable for a particular experiment. The minimum depth for spectral measurements would require (i) sufficient absorber depth so that the primary particle interacts at least once and (ii) enough absorber ($\geq$ 10 radiation lengths) beyond the interaction so that ensuing electromagnetic cascades develop sufficiently well so that their energy content can be measured. The energy resolution of a thin calorimeter defined in this way will depend on fluctuations in the energy transferred (inelasticity) to neutral pions in the interaction. Our use of the term "thin calorimeter" is not very stringent. The calorimeter used in Ref. 8 approaches the minimum possible depth and is strictly classified as thin. In previous cosmic ray exposures,[1-3] the calorimeters are thin in comparison to the ones used at accelerators.

The intrinsic resolution of a deep calorimeter is limited by fluctuations in the fraction of the primary energy going into nuclear disintegrations E_{dis} of the target nuclei. As illustrated in Fig. 2 for a 3.5 λ(proton interaction lengths) calorimeter, this fraction decreases with increasing energy. For a thin calorimeter the amount of E_{out} leaking out the bottom of the absorber plays a crucial role. The example in Fig. 2 indicates that the fractional energy leakage is more the higher the primary energy. The total unmeasured energy is the sum of the disintegration energy and energy leaking out the bottom. It can be seen from the top curve in Fig.

2 that the total unmeasured energy does not drastically change with energy.

Since the energy resolution depends among other things on the total unmeasured energy, the energy resolution for a thin calorimeter will remain approximately constant over two or more decades in energy. This is illustrated in Fig. 3 where the dependence of σ on primary energy is shown for two calorimeter depths. This figure represents accelerator measurements with a tungsten calorimeter of about 1000 g/cm^2 total depth.[20] Notice the similarity between the shapes of the curve for the half-depth energy resolution from Fig. 3 and the curve for the total unmeasured energy in Fig. 2. The same similarity exists between the full-depth energy resolution from Fig. 3 and the curve for the nuclear disintegration energy in Fig. 2.

The data shown in both Figs. 2 and 3 are for events in which the first interaction occurred near the top of the calorimeter. In Fig. 4 is shown a comparison of the resolutions for all incident events, and the subset of events for which the first interaction occurred near the top of the calorimeter. The resolutions are given as a function of the calorimeter depth t for 300 GeV primary protons. It is seen that for both curves the resolution improves with increasing depth, but this improvement is less for particles which interacted near the top. If the depth is sufficiently large, there is not much difference in the resolution for the two cases. With a deep calorimeter it matters very little where the first interaction occurs. However, for a thin calorimeter reasonable energy resolution can be obtained only if the particles have interacted and the subsequent electromagnetic cascades have developed.

In effect, a thin calorimeter measures the energy deposited by the first interaction of the primary particle. Therefore, its use for cosmic

ray energy spectra measurements would result in the spectra being determined from a subset of the primary events. Knowledge of the interaction cross section and inelasticity would be required to obtain the true flux from this subset.

3. Analytical Arguments

The energy spectrum measured with a particular detector, in our case an ionization calorimeter, is a convolution of the primary spectrum and the energy resolution function of the apparatus. Let E represent the primary energy of a number N(E) of events between E and E + dE, and S represent the represent the measured signal which is suitably normalized so that $< S > = E$ for monoenergetic input. If the events of a primary spectrum from the interval between E and E + dE are distributed in S according to the distribution f(E,S)dS, then we will call the normalized density function f(E,S) the "apparatus function". For a primary energy spectrum N(E)dE incident upon this detector, the signal spectrum actually registered is given by

$$N'(S)dS = \int_{E=0}^{E\to\infty} N(E)\, f(E,S)\, dS\, dE \qquad (3)$$

We want to apply this quite general statement to the special problem of measuring power law spectra of the form given in Eq. 1. First we introduce the new variable

$$y = \frac{S}{E} \qquad (4)$$

and assume that the density function g(y) is normalized according to

$$\int_0^\infty g(y)dy = 1, \text{ with } f(E,S) = g(S/E)/E \qquad (5)$$

Thus g(y) is an energy independent function which relates to the apparatus function in a simple way. This is not necessarily a good assumption, particularly not for magnetic spectrometers or Cerenkov counters where the spread of the apparatus function varies rapidly with energy. However, in case of an ionization calorimeter, where the spread is mainly due to the nuclear interaction properties and the inelasticity distribution, this is a fair assumption which is corroborated by experimental results. If we introduce Eqs. 4 and 5 into Eq. 3, we obtain

$$N'(S)dS = dS \int_{y=o}^{\infty} N(S/y)\ g(y)\frac{dy}{y}. \tag{6}$$

Therefore, only the primary spectrum density function $N(E) = N(S/y)$ still contains the variable S under the integral. Since the density function N(E) is of the form given in Eq. 1, we can rewrite Eq. 6 as

$$N'(S)dS = dS\ S^{-\gamma}\ K \int_{y=o}^{y \to \infty} y^{(\gamma-1)} g(y)dy. \tag{7}$$

This simple results shows that the shape of the primary spectrum is reproduced by the detector signal, but with the normalizing constant changed by the factor

$$M = \int_{y=o}^{y \to \infty} y^{(\gamma-1)}\ g(y)dy. \tag{8}$$

Obviously this holds for any shape of the apparatus function f(E,S) as long as Eqs. 4 and 5 are satisfied and provided $< S > = E$.

In general, calorimeter signals are not directly proportional to the primary energy. As discussed in more detail in Sec. 5, calorimeter signals S are more accurately given by

$$< S > = \alpha E^{\beta}$$

where α and β depend on the calorimeter depth but are independent of energy for any particular calorimeter. Following the above arguments, using Eq. 9 instead of $< S > = E$, we obtain for the signal spectrum

$$N'(S)dS = \frac{\alpha}{\beta}^{\frac{\gamma-1}{\beta}} KS^{-(\frac{\gamma-1}{\beta}+1)} dS \int_{y=0}^{y \to \infty} y^{(\frac{\gamma-1}{\beta})} g(y)dy. \qquad (10)$$

This is again a power law, but with the exponent of the integral spectrum modified by the factor $1/\beta$. However, in practice one can avoid this situation by converting the calorimeter signal to energy using the inversion of Eq. 9. If α and β are known from accelerator calibrations and/or Monte Carlo calculations, then the spectrum obtained from the energy measurement E_m, where

$$E_m = (\frac{S}{\alpha})^{\frac{1}{\beta}} \qquad (11)$$

will reproduce the primary spectrum. This case is, in fact, exactly analogous to the discussion leading to Eq. 7. Therefore, if the primary spectrum is a power law and the apparatus function does not change with energy, then the signal spectrum will also be a power law with the same exponent but with a different normalization. We should note that if $\gamma \geq 1$, the modified normalization integral M (Eq. 8) has a finite value for physically reasonable density functions g(y), whereas in case of $\gamma < 1$, the integral may or may not be divergent, depending on the exact functional behavior of the density function g(y) near y = 0. In practice, of course, we do not expect an energy spectrum with $\gamma < 1$.

4. Gaussian Distributions for Energy Resolution

The above analytical arguments are applicable only if the energy resolution distributions do not change with energy. In this section

we present results from a Monte-Carlo study of the effect of energy resolutions on measurements of spectral indices.

For simplicity we have chosen Gaussian distributions for the energy resolution. This is a reasonable approximation for calorimeters of moderate thickness. In addition to using distributions whose widths did not change with energy, we considered separately cases where the widths increased and decreased.

The method consisted basically of calculating the number of particles in different energy bins over two decades in energy, using five bins per decade. The exact number of particles in each bin was calculated using the chosen differential power law spectrum. Statistical fluctuations were applied to determine the number of particles in each bin. This procedure accounts for the fact that the spectrum being observed at any one time is actually a statistical sample of the true primary spectrum. Finally, the existing spectrum was convoluted with the energy resolution function of the detector. This was accomplished by randomly selecting the energy for each observed particle from the distribution function representing the energy resolution. The mean of the distribution was taken to be the mean energy of the particles in the energy bin containing the observed particle. Using the mean energy in the bin instead of the actual energy of the particle reduced the computer storage and calculation time without significantly affecting the results.

Calculations were carried out for values of the spectral index γ ranging from 2.0 to 2.8. The measured differential spectral indices appear to fall in this range. For each index several widths of the energy resolution distributions have been considered. The distributions were

chosen to have standard deviations which cover the range of energy resolutions obtained from actual experiments. The effect of a low energy cutoff (e.g. geomagnetic) was tested by successively omitting low energy bins in carrying out least squares fits to the convoluted spectra.

In Fig. 5 are shown the results obtained fom the case where σ (= 0.3, 0.4, and 0.5) remains constant with energy. Each graph shows the value of the measured (calculated) spectral index γ_{meas} as a function of the true index γ_{true}. The solid line of unit slope indicates equal values of γ_{meas} and γ_{true}. The different sets of plotted points show the results of weighted least squares fits to the convoluted spectra. The open circles are for fits to all energy bins (L_0 =1), while the X's and the solid circles represent fits with the lower energy bins omitted (L_0 = 2 and 3). The graphs show that for all three resolutions the value of γ_{meas} agrees with γ_{true} for the entire range of indices calculated, provided the two lowest energy bins are omitted. For each spectral index value we have performed a single calculation representing a single experiment. The deviation of the solid points from the solid line represents the error one can expect in performing a single measurement of a primary spectrum.

It should be emphasized that events in the individual energy bins of the convoluted spectrum do not represent the actual number of primary events in those bins. As shown in Ref. 8, the major contribution to a particular bin stems from events of somewhat lower primary energies. This results from particles suffering large energy loss, and therefore falling into a higher bin where there are fewer particles because of the rapidly decreasing flux at higher energies. Since the contribution to a particular bin from higher energies is small in comparison to the

contribution from lower energies, the measured flux is higher than the true flux. However, there is an equilibrium in the relative number of particles having apparent energies higher or lower than the true energy. This equilibrium causes the convoluted flux to have the same relative energy dependence as the primary flux, i.e., the same spectral index, as long as boundary effects are excluded. This is illustrated in Fig. 6 where the fluxes are given as a function of energy for an input spectrum index $\gamma = 2.6$ and an energy resolution $\sigma = 0.4$. The sharp low energy cutoff of the input spectrum destroyed the equilibrium, and consequently the convoluted flux is distorted near the low energy cutoff. For this reason it was necessary to omit the lowest energy bins in Fig. 5 in order to obtain the correct values for the measured spectral indices. The number of bins that have to be omitted depends on both the energy resolution and the index of the primary spectrum.

Slowly developing cascades, with the correspondingly large amount of energy leaking out the bottom of a thin calorimeter, will result in a much lower than average energy deposition.[15,23] This causes the energy resolution distributions to be not strictly Gaussians but rather more like Gaussians with tails extending back toward zero. In Fig. 7 are shown the results for the case where the energy resolution distributions have lead tails. Again the overall resolutions considered are 0.3, 0.4 and 0.5, independent of energy. In order to simulate the lead tail, the sum of two Gaussian distributions was used. The main distributions, corresponding to more fully developed cascades, were used to select the energies of 84% of the events, while 16% of the events had energies selected from the wider (lead tail) distribution. The resolution σ_2

of the lead tail distribution was taken to be three times as large as the resolution σ_1 of the most prominent distribution. The mean μ_2 of the lead tail distriwas set equal to $\mu_1 - 2\sigma_1$, where μ_1 was the mean of the main distribution. It can be seen from Fig. 7 that the lead tail does not seriously affect spectral index measurements. The main consequence of the lead tail is an increased disturbance in the equilibrium of the convoluted spectrum so that more particles are assigned energies below the low energy cutoff. This statement would not change if different percentages of events had been used in the two parts of the hybrid lead-tail distributions. We conclude, therefore, that asymmetric energy resolution distributions can also be reliably used for power law spectral measurements provided proper caution is exercised near the cutoff energies.

So far we have considered only distributions whose shapes do not change with energy. In practice, no device can measure all energies with the same accuracy, so the shapes will in general change with energy. In order to test the effect of energy dependent resolutions, we considered both increasing and decreasing widths of the distributions with energy. The results are illustrated in Fig. 8 for three monotonically changing energy resolution functions. The solid circles represent approximations for the resolution obtained with a moderately thin calorimeter[2,4], i.e., a slow increase in width as the primary energy increases. The solid triangles correspond to a deep calorimeter[19,20], where the distribution widths significantly decrease with energy. The crosses represent distributions which become significantly wider with increasing energy. This latter case is too extreme for thin calorimeters, but may be indicative of other types of energy measurement techniques.

It is clear from Fig. 8 that energy resolutions which drastically change with energy will result in incorrect measurements of power law spectral indices. If the resolution greatly improves as energy increases the measured spectra will be too steep, while resolutions getting much worse with energy will result in spectra that are too flat. The deviation of the measured index γ_{meas} from the true index γ_{true} is larger for steeper spectra. This deviation is also greater the more rapid the energy dependence of the resolution. If the resolution is a slowly varying function of energy, as in the case of a thin calorimeter, the effect on the spectral index will be small. This is indicated by the proximity of the solid circles to the solid line drawn in Fig. 8.

5. Monte-Carlo Cascade Simulations for Energy Resolution

In this section we present results which do not rely on the assumption of Gaussian distributions for the energy resolution. Instead, we have carried out a complete simulation of an experiment to measure spectral indices. This simulation consisted of using a detailed Monte-Carlo program to calculate the cascade developments for an isotropic flux of protons whose energies were selected from a power law distribution. The calculations were specifically for a 3.5λ deep iron calorimeter[2,4] flown in two balloon exposures. The Monte-Carlo events were analyzed by the same method used for the flight data. The Monte-Carlo model has been compared with a variety of measurements using different calorimeter configurations and absorbers. The fluctuation distributions of the energy loss resulting from these model calculations typically have shapes like Haussian distributions with lead tails similar to the ones used for Fig. 7. The calculations have consistently been in good agreement with measurements. Therefore, it is expected that this simulation technique for checking

the spectral index measurements should also be reliable.

Because of the large amount of computer time required to perform detailed calculations for high energy cascades, it was necessary to use a simplified procedure. Our approach was to generate a set of isotropic proton events whose energies were selected from a uniform distribution in the logarithm of the primary energy. The calculations covered the range 10 - 4000 GeV. A power law spectrum was simulated by weighting each calculated event according to the chosen input spectrum. This technique, of course, does not accurately represent the statistical errors associated with a primary spectrum but it does permit a spectrum simulation without calculating an enormous number of events. Furthermore, the same calculated events can be used to simulate any arbitrary input spectrum.

The convolution of the input spectrum with the calorimeter resolution function was obtained in the following ways. First, the number N_j of calculated events in various energy bins was determined, using 5 bins per decade for the input Monte-Carlo energies E_i. Next the energy E_m measured by the calorimeter for each event was determined from the algorithm (discussed below) used to convert the measured signal to primary energy. The weighting factor used for each event having signal E_m was $K E_i^{-\gamma}/N_j$, where N_j was the number of events actually calculated for the energy bin in which the true energy E_i was located. The convoluted flux was then given directly by binning this weighted flux in terms of E_m, also using 5 bins per decade.

A schematic diagram of the GSFC calorimeter used in this simulation is shown in Fig. 9. It consisted of 7 modules, each 0.5 proton interaction lengths thick, with a total depth of 3.5 interaction lengths. The modular structure easily affords testing calorimeters of different depths. By

neglecting signals in the downstream modules we have considered depths from 2.0 to 3.5 interaction lengths.

The response of the calorimeter to particles of primary energy E_o is well represented by the relation

$$\langle \Sigma_k N \rangle = \alpha_k \, E_o^{\beta_k}$$

The calorimeter signal $\Sigma_k N$ is the summed number of cascade particles in k modules, where the summation begins with the module in which the first interaction occurred. The parameters α and β used for this work were $\alpha_7 = 6.4$, $\beta_7 = 0.97$, $\alpha_4 = 5.7$ and $\beta_4 = 0.9$. These values were obtained from a least squares fit to a plot of log ΣN vs log E_i for all the 2087 cascades calculated in detail as the first step in this simulation procedure. They are valid for an isotropic flux of protons whose trajectories are restricted to pass through both the top and bottom of the calorimeter. Therefore, for each calorimeter depth (k modules) the estimated energy E_m^k assigned each particle was determined from the algorithm

$$E_m^k = \left(\frac{\Sigma_k N}{\alpha_k}\right)^{\frac{1}{\beta_k}}$$

Our results for energy spectra measurements, using the cascade simulations for primary protons, are given in Figs. 10, 11, and 12. Figure 10 is for a simple power law, while Figs. 11 and 12 are for a power law with a bend and an energy dependent spectral exponent, respectively. In each figure the logarithm of the differential flux is shown as a function of primary energy E_o. The circles represent the Monte-Carlo input flux, the crosses represent the flux obtained using 4 modules for the energy measurement, and the triangles represent the flux using energy measurements from all 7 modules. Notice that the flux from 4 modules is higher than the input flux for energies considerably greater than the cutoff energy (bin 6). The reason for this effect was explained above in relation to

Fig. 6. The flux obtained from 7 modules is less than the input flux because of the smaller total number of events that pass the selection criterion: Not all events had cascades developing in all 7 modules. However, if suitably normalized, this flux would also be greater than the input flux.

It seems to be clear from Figs. 10, 11 and 12 that the calorimeter signals are capable of reproducing the input spectrum, whether the spectrum is a simple power law, a power law with a bend, or an energy dependent function. This is true for energy measurements using either 4 modules or 7 modules of the calorimeter. This result substantiates our earlier conclusion from Fig. 6 that a moderate energy dependence of the energy resolution function will not greatly distort spectral measurements. It should be pointed out here that the proton energy resolution for 4 modules of the GSFC calorimeter ranges from 32% to 38% as the primary energy goes from 17.6 GeV to 1000 GeV. For the same energy range the resolution for 7 modules changes from 20% to 23%.

In calculating the results given in Fig. 11, we arbitrarily set the abrupt change in the spectral index from 2.5 to 3.0 to occur at 500 GeV. This energy value was chosen in order to have data for several energy bins on either side of the kink. Qualitatively, the results would not differ regardless of where the index change occurred. However, as a practical matter, it would be necessary in an experiment to have energy measurements over about one decade in energy above such a kink in order to detect it.

The necessity of a large energy range is even more acute in case of an energy dependent spectral exponent. In fact, straight lines

exemplifying simple power laws, provide very good fits to any 5 points (one decade) of the flux presented in Fig. 12, as long as bins near the low energy cutoff are omitted. Experimentally, for example, one might interpret that energy dependent spectral exponent as a spectrum consisting of different power law indices on either side of a kink at about 500 GeV. Consequently, differentiation between a spectrum with a bend and an energy dependent exponent requires at least three and preferably four decades of energy coverage.

6. Conclusion

Evidence has been presented to show that a thin ionization calorimeter can be used to determine the energy spectra of high energy cosmic rays. Since many primary particles may penetrate a thin absorber without interacting, a thin calorimeter is useful only for measuring energies of particles that interact near its top. Consequently, one must know the relevant interaction cross sections in order to determine absolute particle fluxes. Since many cross sections measurements have been, or can be, made using the high energy accelerators now available, this does not in principle limit the use of thin calorimeters for energy spectra measurements.

Regarding the effect of poorer energy resolution on measured energy spectra, it has been shown that the index of a single power law spectrum can be obtained with energy resolutions of 50% or worse. In order to detect structure such as kinks and bumps in the spectra it is desirable to have both good energy resolution and good statistics. A bump in a spectrum which has a width smaller than the energy resolution will appear smeared out in the measurements. An abrupt kink will also tend to smear out more as the energy resolution decreases. If a spectrum really consists

of two separate power laws, it is necessary that good statistics be obtained for events with energies substantially greater than the energy where the kink occurs. The coverage of a large energy range in a single experiment is necessary to determine whether the primary spectral exponents are actually energy dependent.

In experiments involving the low fluxes of very high energy cosmic rays one must invariably make a compromise between the accuracy of energy measurments and apparatus collecting power. All calorimeters used in cosmic ray experiments near the top of the atmosphere have been in fact, relatively thin.[1,2,4,8] The one used by Schmidt et al.[8] approaches the minimum allowable depth as defined in Sec. 2. There are alternate energy measuring techniques known that allow instruments with large geometry factors to be built such as gas Cerenkov detectors and transition radiation detectors. These techniques suffer from the fact that the dynamic range is relatively narrow for each individual instrument and a spectrum would have to be pieced together using several different techniques. In piecing data together from several instruments one can never rule out that systematic errors enter that, while giving satisfactory values for the fluxes at different energies, might partially obscure the information that is contained in the detailed knowledge of the spectral shape. A thin ionization spectrometer seems to be the only currently practical means for determining the shape of cosmic ray particle energy spectra over a very large dynamic range in one single experiment. Deeper calorimeters provide accurate energy measurements, but being subject to always present and cost limitations, the deeper calorimeters have smaller collecting area solid angles. Our studies

have shown that measurements of the spectra of high energy particles would be more affected by the low numbers of events collected, thereby limiting the energy range covered, rather than by the accuracy of the energy measurements of those events. For this reason, a thin ionization calorimeter should provide a viable means of answering timely questions on the energy spectra and composition of high energy cosmic rays.

References

1. W. K. H. Schmidt, K. Pinkau, U. Pollvogt, and R. W. Huggett, Phys. Rev. 184, 1279 (1969)

2. M. J. Ryan, J. F. Ormes, and V. K. Balasubrahmanyan, Phys. Rev. Letters 28, 985 (1972)

3. E. Juliusson, P. Meyer, and D. Muller, Phys. Rev. Letters 29, 495 (1972)

4. V. K. Balasubrahmanyan and J. F. Ormes, Astrophys. J. 186, 109 (1973)

5. L. H. Smith, A. Buffington, C. F. Smoot, L. W. Alvarez, and W. H. Wahlig, Astrophys. J. 180, 987 (1973)

6. W. R. Webber, J. A. Lezniak, J. C. Kish, and S. V. Damle, Nature 241,

7. R. L. Golden, J. H. Adams, Jr., C. L. Deney, G. D. Badhwar, T. M. K. Marar, H. H. Heckman, and P. J. Lindstorm, Astrophys. J. 192, 747

8. W. K. H. Schmidt, K. Atallah, T. F. Cleghorn, W. V. Jones, A. Modlinger, and M. Simon, Astron. and Astrophys. 46, 49 (1976)

9. N. L. Grigorov, N. A. Mamontova, I. D. Rappaport, I. A. Savenko, V. V. Akimov, V. E. Nesterov, and B. M. Yakovlev, Conference Papers, 12th International Conference on Cosmic Rays, Hobart, Tasmania, Vol. 5, p. 1746 (1971)

10. W. V. Jones, K. Pinkau, U. Pollvogt, W. K. H. Schmidt, and R. W. Huggett, Nucl. Instrum. Methods 72, 173 (1969)

11. E. B. Hughes, R. Hofstadter, W. L. Lakin, and I. Sick, Nucl. Instrum. Methods 75, 130 (1969)

12. W. V. Jones, Phys. Rev. 187, 1868 (1969)

13. W. V. Jones, Phys. Rev. D 1, 2201 (1970)

14. L. W. Jones, A. E. Bussian, G. D. Demeester, B. W. Loo, D. E. Lyon, Jr., P. V. Ramana Murthy, R. F. Roth, P. R. Vishwanath, J. G. Learned, D. D. Reeder, R. J. Wilkes, K. N. Erickson, F. E. Mills, and B. Cork, Nucl. Phys. B 43, 477 (1972)

15. J. Engler, W. Flauger, B. Gibbard, F. Monnig, K. Runge, and H. Schopper, Nucl. Instrum. Methods 106, 189 (1973)

16. F. Sichan, M. LaPointe, J. MacFall, A. Stottlemeyer, R. W. Ellsworth, and G. B. Yodh, Conference Papers, 13th International Conference on Cosmic Rays, Vol. 3, P. 2129 (1973)

17. H. Whiteside, C. J. Crannell, H. Crannell, J. F. Ormes, M. J. Ryan, and W. V. Jones, Nucl. Instrum. Methods 109, 375 (1973)

18. T. A. Gabriel and J. D. Amburgey, Nucl. Instrum. Methods 116, 333 (1974)

19. B. C. Barish, J. F. Bartlett, D. Buchholz, T. Humphrey, F. S. Merritt, Y. Nagashima, F. J. Sciulli, D. Shields, H. Suter, G. Krafczyk, and A. Maschke, Nucl. Instrum. Methods 116, 413 (1974)

20. L. W. Jones, J. P. Chanowski, H. R. Gustafson, M. J. Longo, P. L. Skubic, J. L. Stone, B. Cork, Nucl. Instrum. Methods 118, 431 (1974)

21. Antonio Baroncelli, Nucl. Instrum. Methods 118, 445 (1974)

22. D. L. Cheshire, R. W. Huggett, W. V. Jones, W. K. H. Schmidt, and M. Simon, Conference Papers, 14th International Conference on Cosmic Rays, Munich 1975, Vol. 9, p. 3233

23. The Proceedings of the Calorimeter Workshop, Fermi National Accelerator Laboratory, Batavia, IL, May 1975, M. Atac, Editor, contains recent results from many authors as well as additional references.

Figure Captions

Fig. 1 (a) Energy spectra of protons and helium nuclei.[2]

(b) Energy spectra for heavier nuclei.[3]

Fig. 2 Typical results for the unmeasured energy in an ionization calorimeter as a function of the primary proton energy E_o. These results are from a Monte Carlo simulation of the cascade development for 3.5 λ deep iron calorimeter. (See Sec. 5). Nuclear disintegration energy is represented by E_{dis} while the energy leaking out the bottom is given by E_{out}; the sum $E_{dis} + E_{out}$ constitutes the total unmeasurd energy.

Fig. 3 Energy resolutions for two calorimeter depths as a function of primary energy E_o.[20] The energy measured by the calorimeter is given by E_m. These results are from accelerator measurements with a tungsten calorimeter of 1000 g/cm^2 total depth. The abbreviation HRM represents the "high resolution module" located at the top of the calorimeter.

Fig. 4 Energy resolutions as a function of tungsten calorimeter depth for 300 GeV protons.[20] For the upper curve the location of the first interaction could be anywhere. The lower curve includes only events in which the first interaction occurred in the high resolution module (HRM) at the top of the calorimeter.

Fig. 5 Calculated results for the measured spectral indices γ_{meas} as a function of the true indices γ_{true}. Gaussian distributions were used for the energy resolutions. (a) Relative standard deviation $\sigma = 0.3$, (b) $\sigma = 0.4$, and (c) $\sigma = 0.5$. Weighted least squares

fit for all energy bins is indicated by $L_o = 1$, while $L_o = 2$ is for fit omitting lowest energy bin, and $L_o = 3$ is for fit omitting the two lowest energy bins.

Fig. 6 Typical comparison of the input power law flux with the flux obtained after folding in the energy resolution distributions. The calculated flux has 8645 events below the low energy cutoff.

Fig. 7 Calculated results for the measured spectral indices γ_{meas} as a function of the true indices γ_{true}. Two Gaussian distributions were used to simulate symmetrical energy resolution distributions having lead tails. The overall relative standard deviation σ was taken to be energy independent. The main distribution (σ_1) was used for 84% of the events, and the lead tail distribution (σ_2) for 16% of the events.

Fig. 8 Calculated results for the measured spectral indices γ_{meas} as a function of the true indices γ_{true}. These results are for Gaussian energy resolution distributions which have the indicated energy dependence. The solid line represents equal values of γ_{meas} and γ_{true}. The dashed lines are visual fits to the data.

Fig. 9 Schematic diagram of the iron calorimeter used by the Goddard Space Flight Center. The results in Figs. 10, 11, and 12 were calculated for this calorimeter design.

Fig. 10 Calculated results for the differential fluxes measured with an iron calorimeter of two different depths. The input spectrum was a simple power law with spectral index $\gamma = 2.7$. The measured fluxes were determined from the cascade energy deposited in 4

modules and 7 modules, respectively, of the iron calorimeter illustrated in Fig. 9. Parallel lines were drawn through the calculated points to show that the measured spectral indices, represented by the slopes of the lines, reproduced the input spectral index.

Fig. 11 This plot is the same as Fig. 10, except the input spectrum index was changed from 2.5 to 3.0 at 500 GeV.

Fig. 12 This plot is the same as Fig. 10, except the input spectrum had an energy dependent exponent. Note that, although the data points representing measurements follow the curvature of the input data, straight lines also provide good fits over a single decade (five data points) in energy. Over two decades in energy, two straight lines of different slopes, analogous to Fig. 11, would be a good fit.

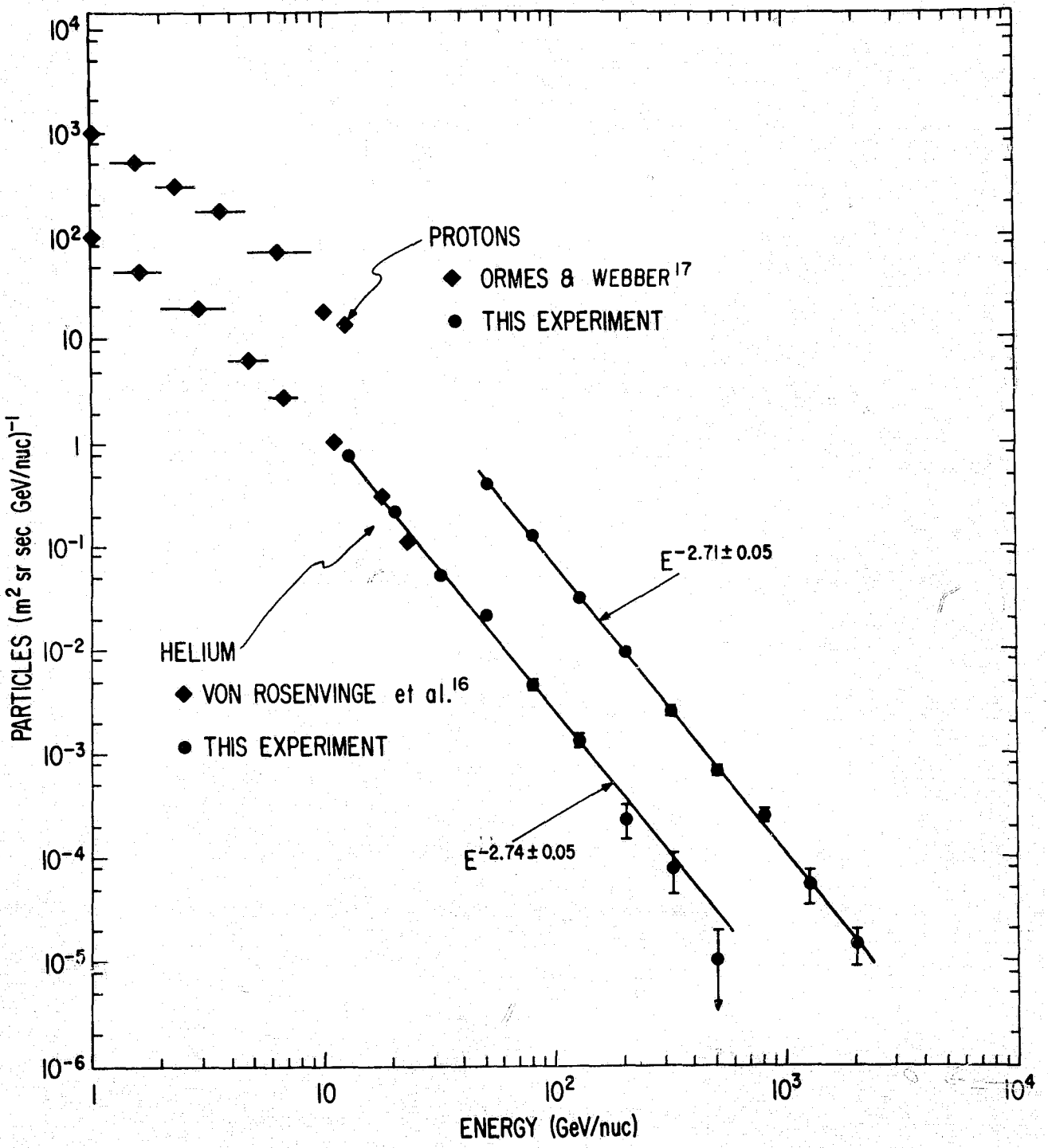

Fig. 1a

PRECEDING PAGE BLANK NOT FILMED

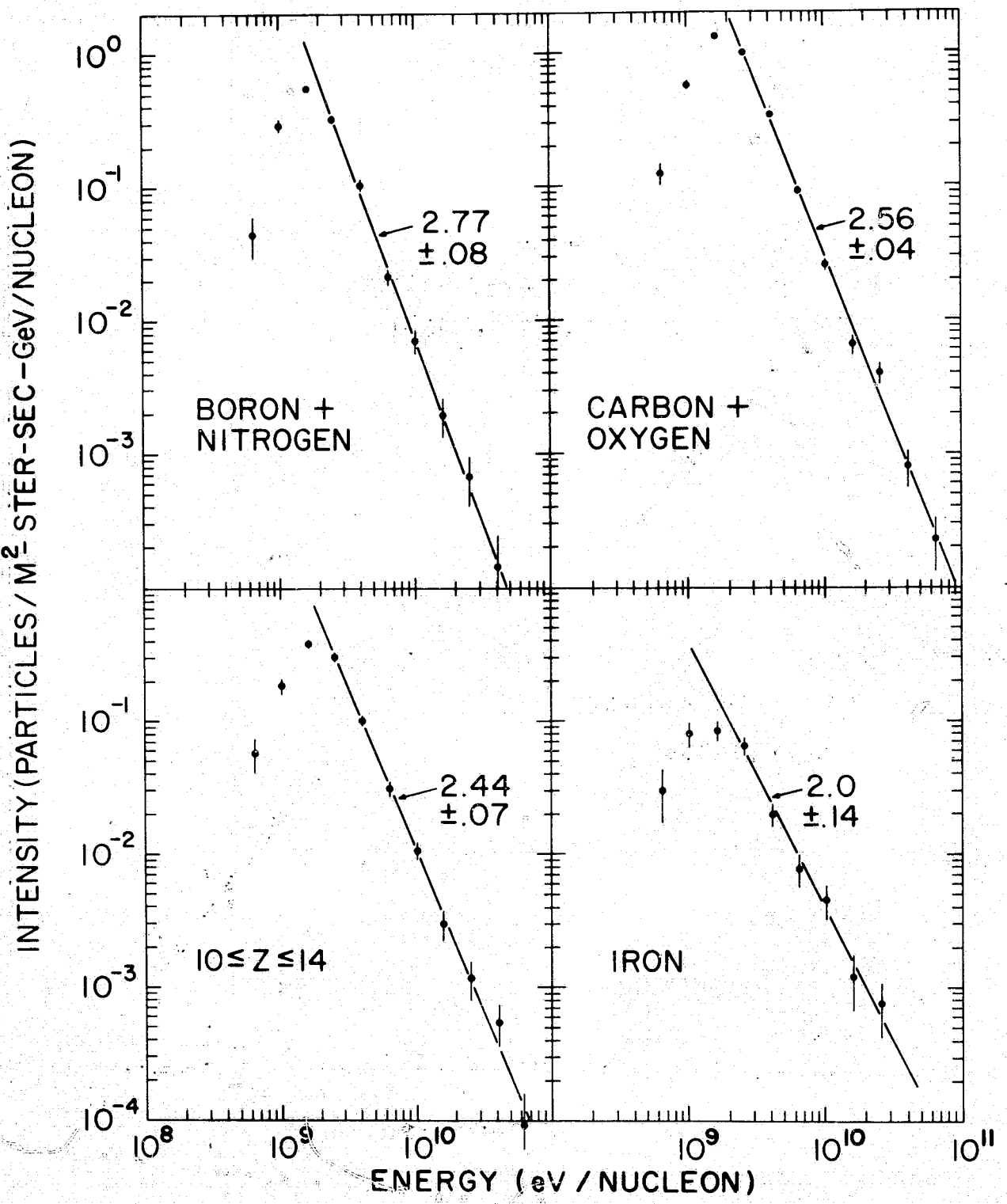
INTENSITY (PARTICLES / M² STER-SEC-GeV/NUCLEON)
ENERGY (eV / NUCLEON)
BORON + NITROGEN
2.77 ±.08
CARBON + OXYGEN
2.56 ±.04
10≤Z≤14
2.44 ±.07
IRON
2.0 ±.14

Fig. 1b

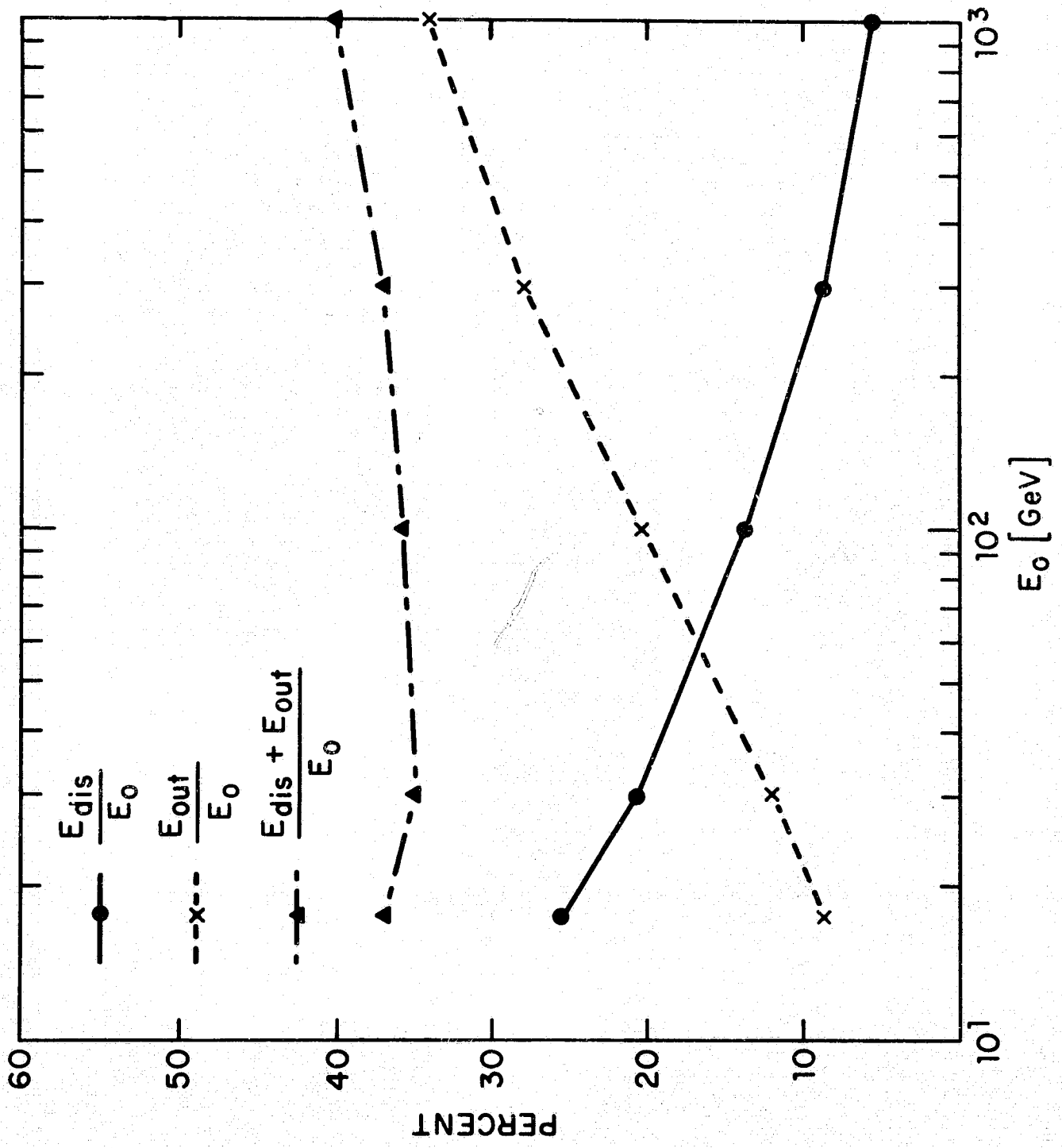
PERCENT
60
50
40
30
20
10
10^1
10^2
10^3
E_o [GeV]
$\frac{E_{dis}}{E_o}$
$\frac{E_{out}}{E_o}$
$\frac{E_{dis} + E_{out}}{E_o}$

Fig. 2

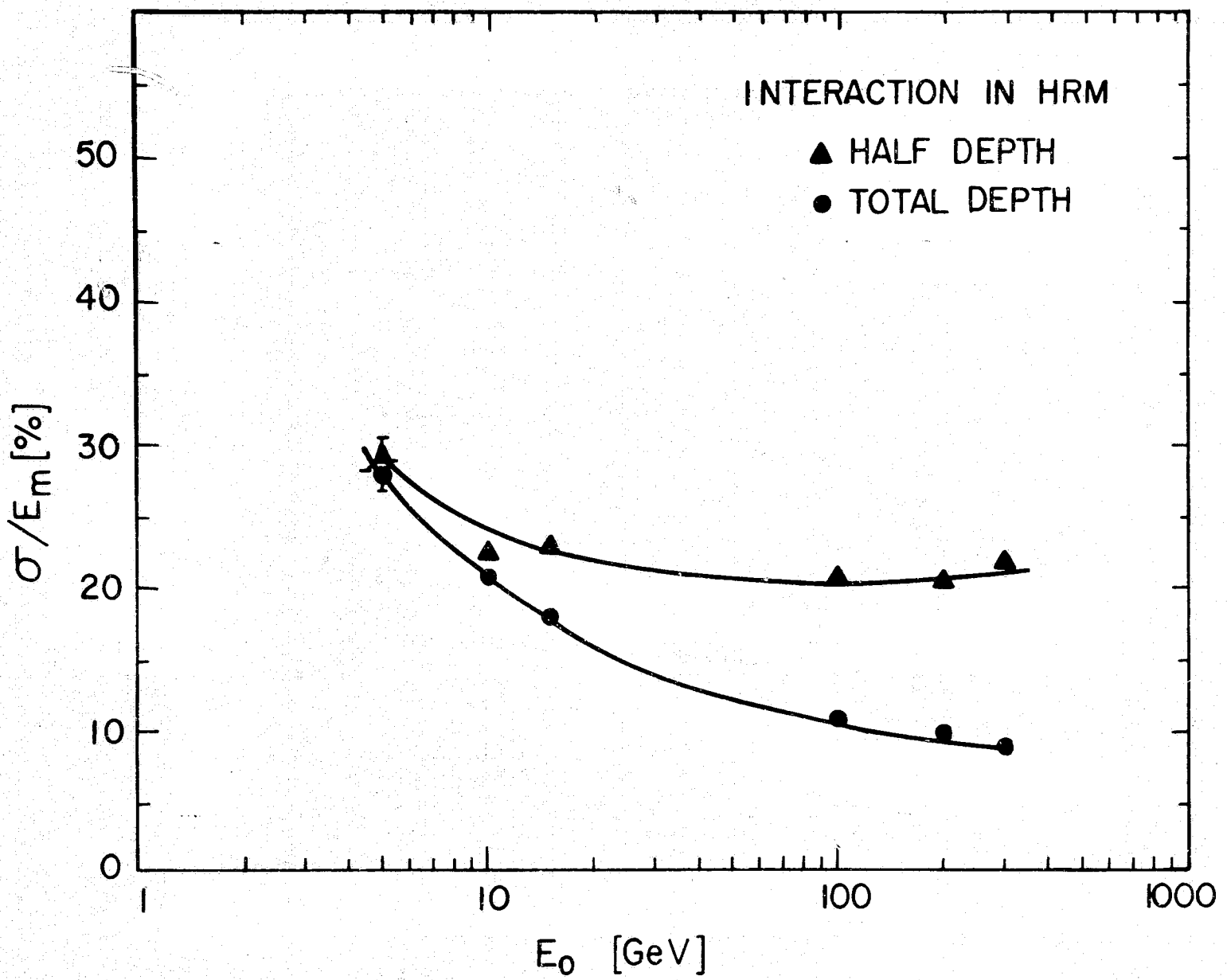
INTERACTION IN HRM
▲ HALF DEPTH
● TOTAL DEPTH
σ/Em [%]
50
40
30
20
10
0
1
10
100
1000
E0 [GeV]

Fig. 3

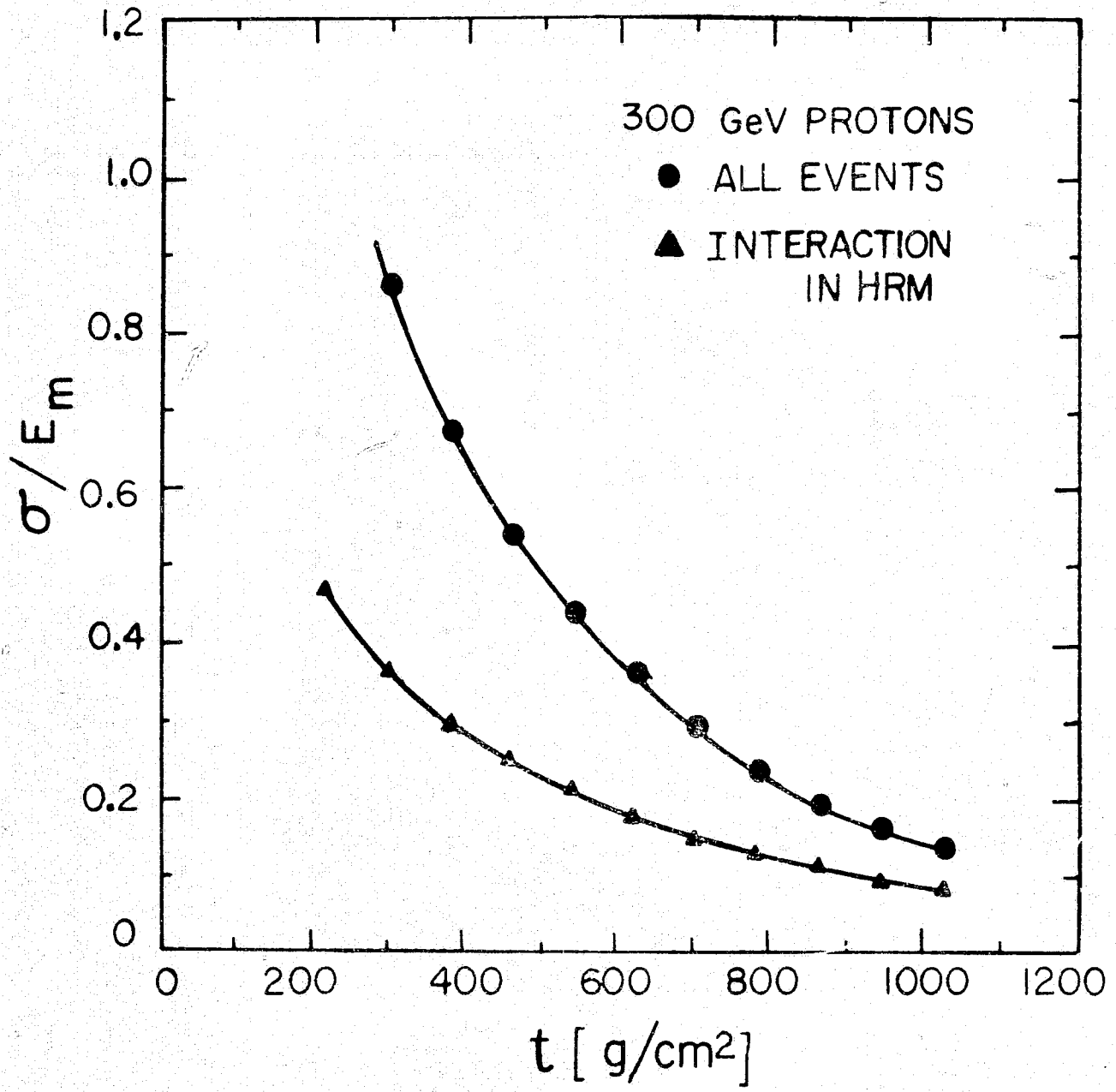
300 GeV PROTONS
ALL EVENTS
INTERACTION IN HRM
σ/Em
t [g/cm²]
0
0.2
0.4
0.6
0.8
1.0
1.2
0
200
400
600
800
1000
1200

Fig. 4

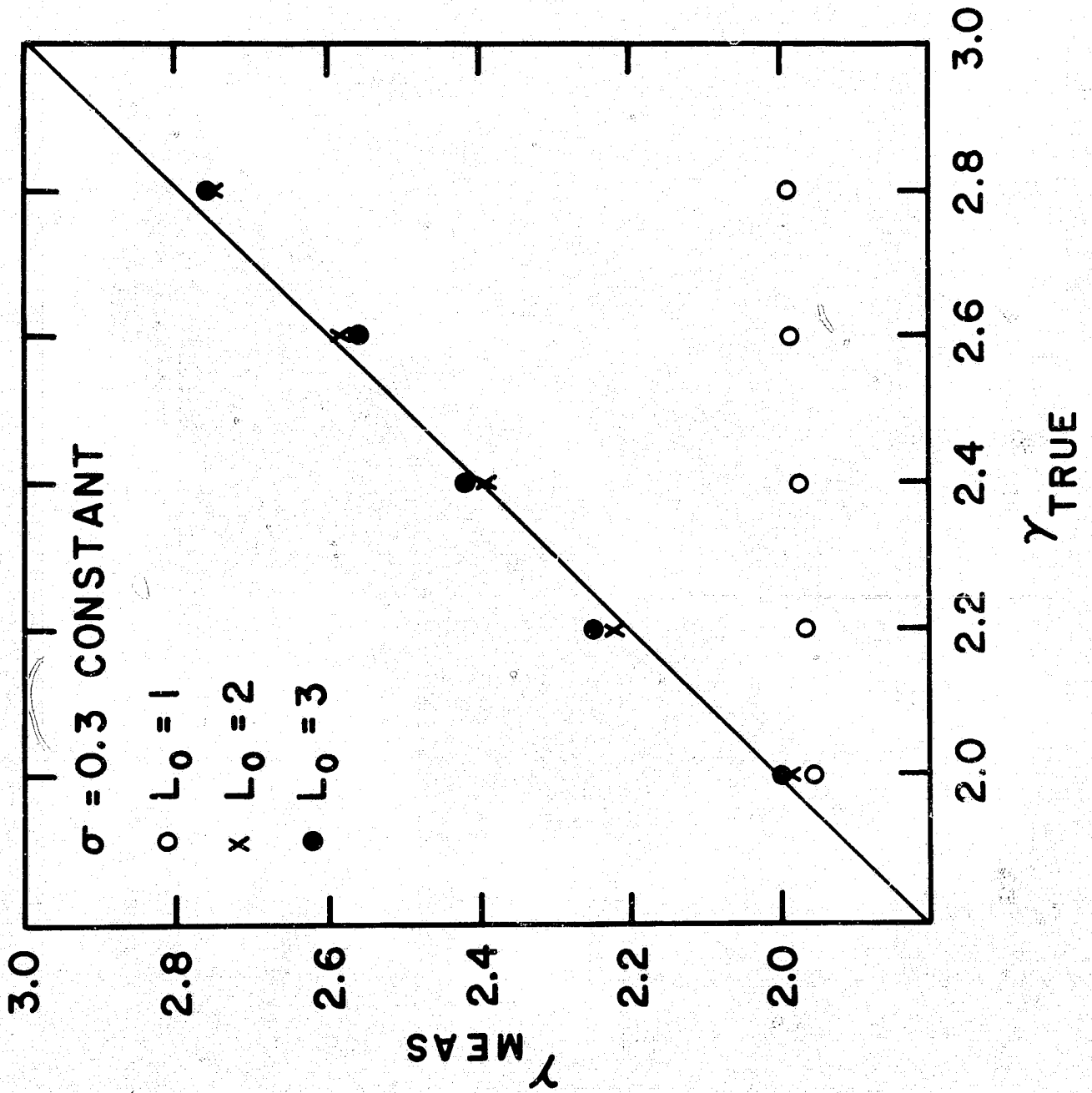
σ = 0.3 CONSTANT
o L_0 = 1
x L_0 = 2
● L_0 = 3
γ_{MEAS}
γ_{TRUE}
3.0
2.8
2.6
2.4
2.2
2.0

Fig. 5a

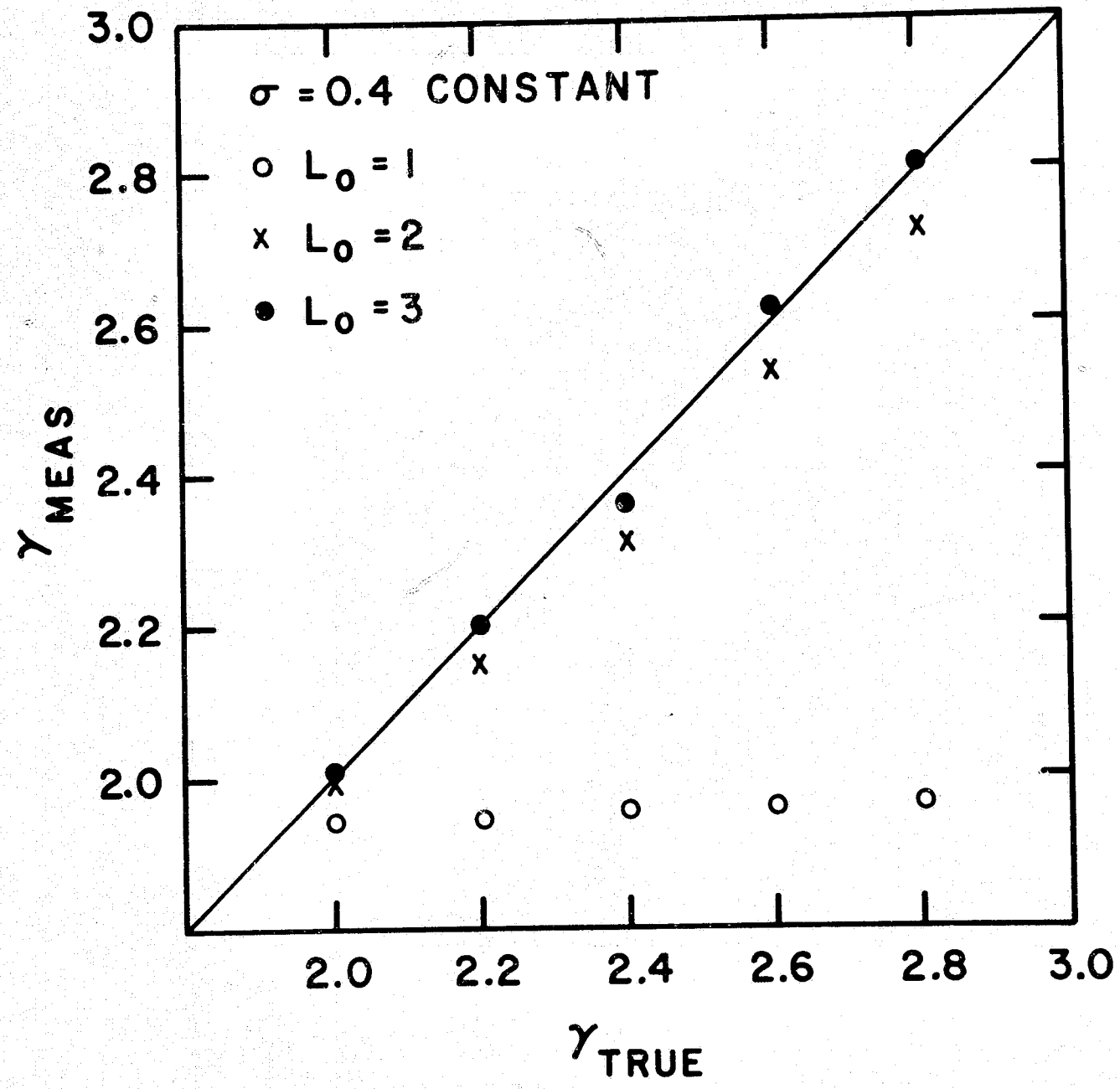
σ = 0.4 CONSTANT
o L_0 = 1
x L_0 = 2
● L_0 = 3
γ_{MEAS}
γ_{TRUE}
3.0
2.8
2.6
2.4
2.2
2.0
2.0
2.2
2.4
2.6
2.8
3.0

Fig. 5b

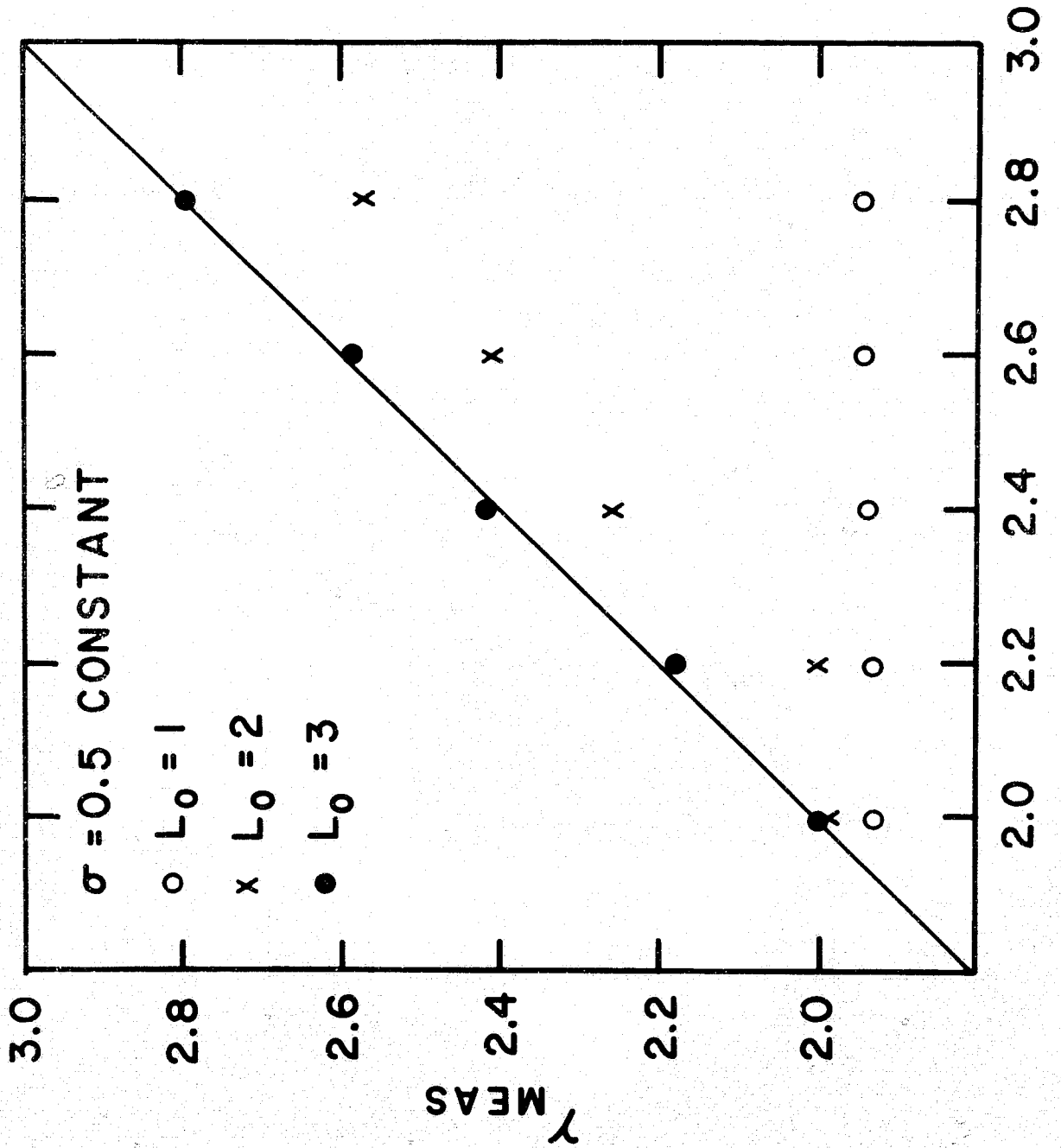
σ =0.5 CONSTANT
o L_o = 1
x L_o = 2
● L_o = 3
γ_{MEAS}
γ_{TRUE}
3.0
2.8
2.6
2.4
2.2
2.0

Fig. 5c

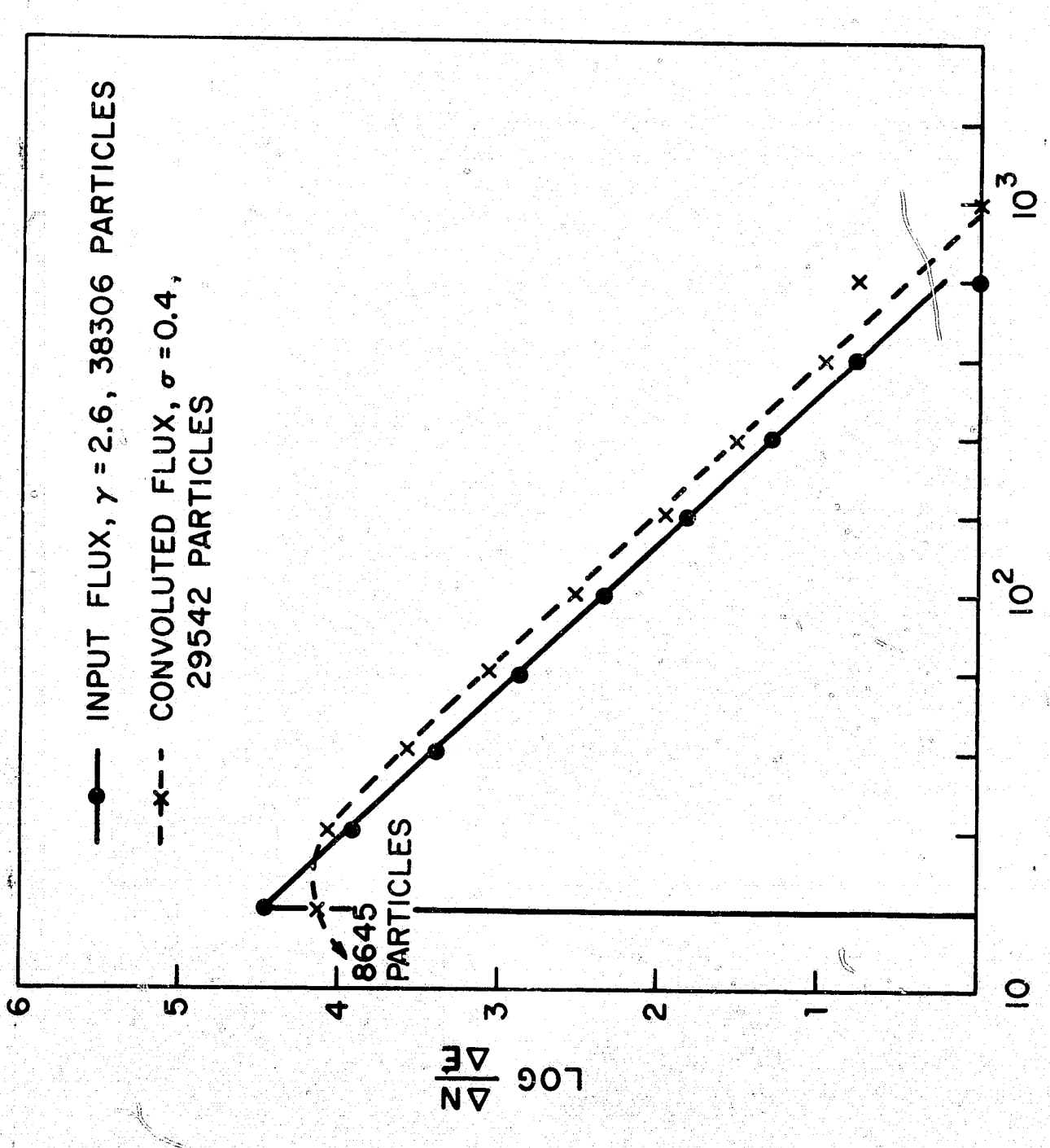
INPUT FLUX, γ = 2.6, 38306 PARTICLES
CONVOLUTED FLUX, σ = 0.4, 29542 PARTICLES
8645 PARTICLES
LOG ΔN/ΔE
E (GeV)
10
10^2
10^3
1
2
3
4
5
6

Fig. 6

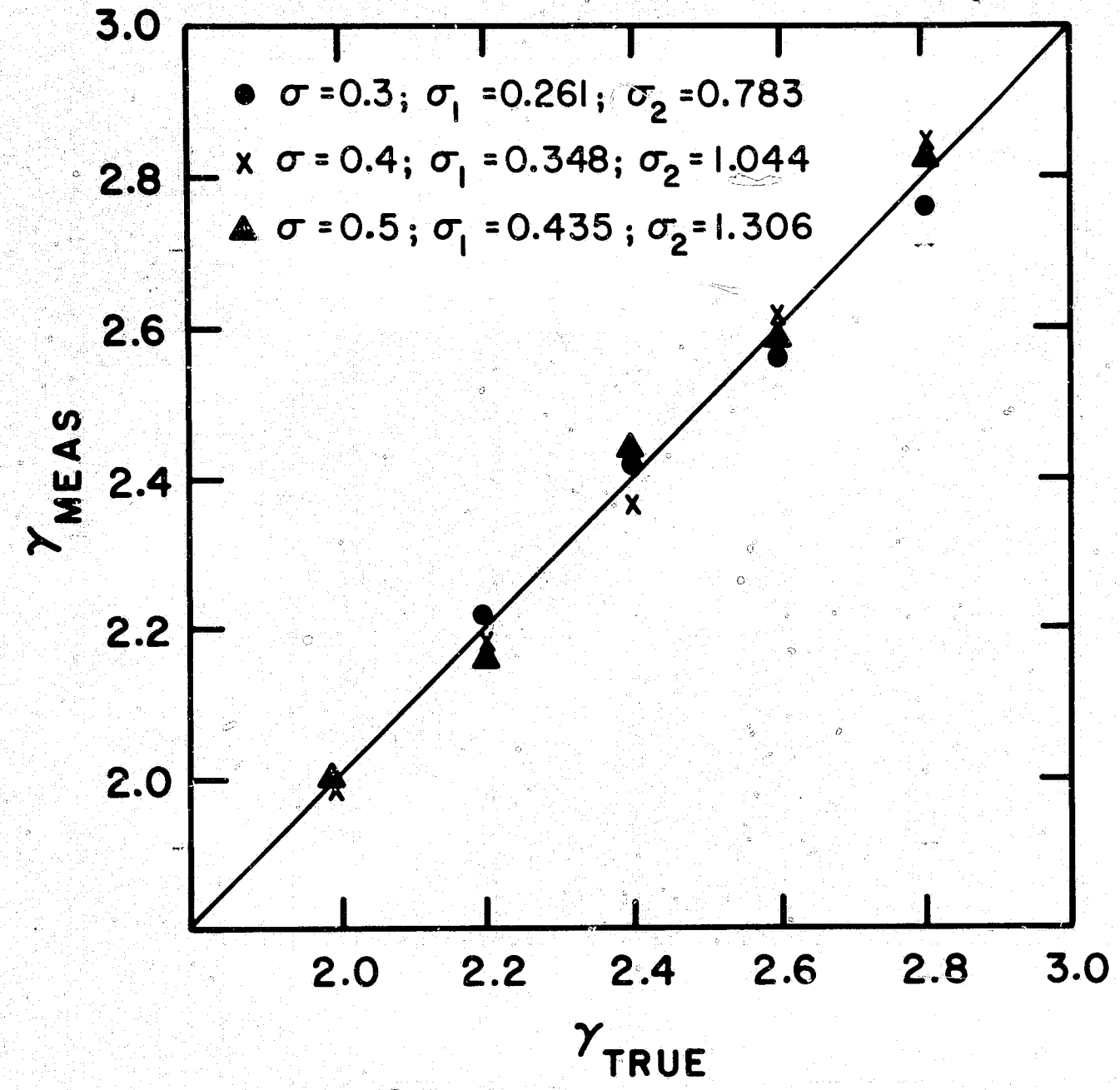
3.0
2.8
2.6
2.4
2.2
2.0
γ_{MEAS}
● σ =0.3; σ_1 =0.261; σ_2 =0.783
x σ = 0.4; σ_1 =0.348; σ_2 = 1.044
▲ σ = 0.5; σ_1 = 0.435; σ_2 = 1.306
2.0
2.2
2.4
2.6
2.8
3.0
γ_{TRUE}

Fig. 7

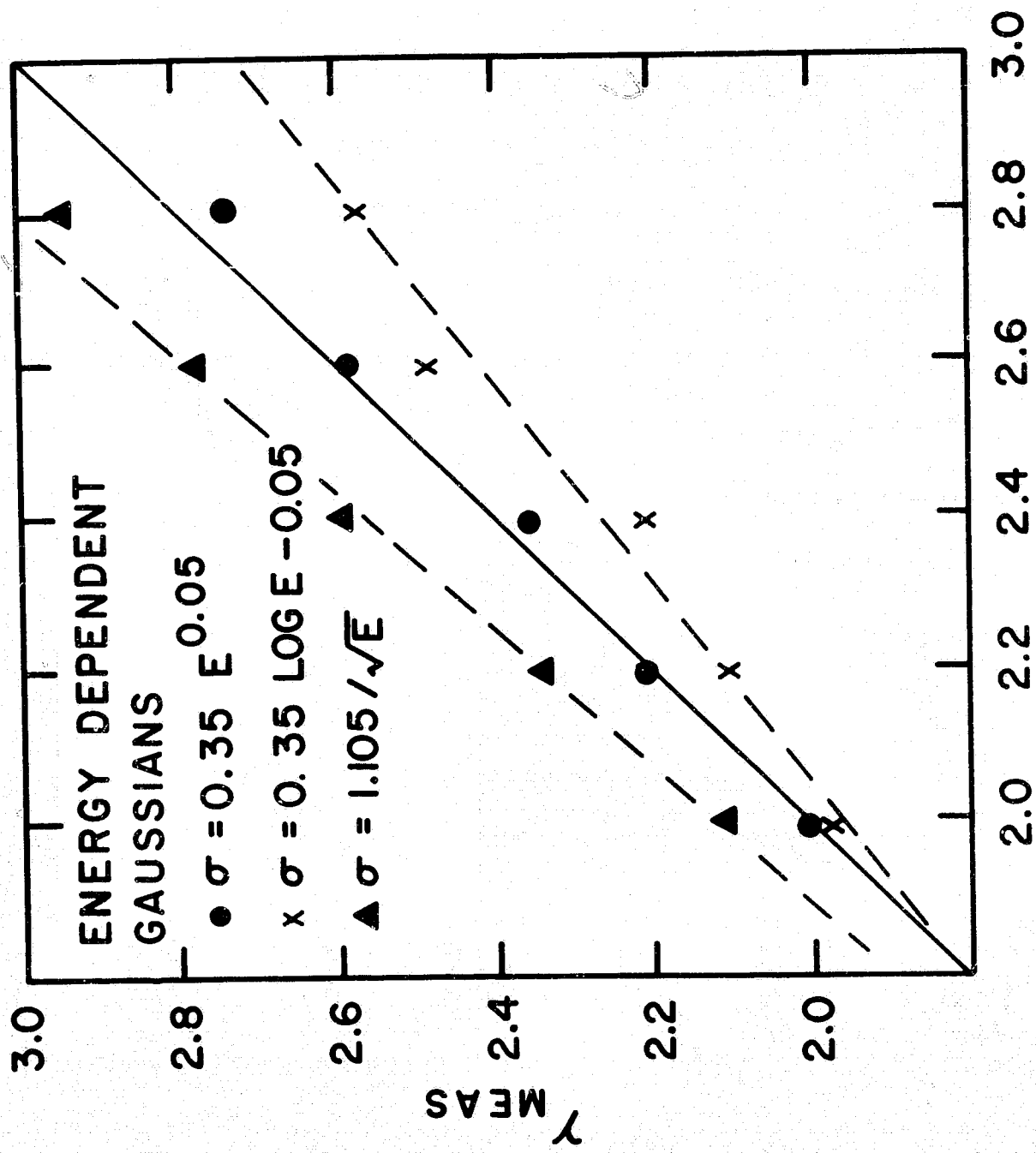
ENERGY DEPENDENT
GAUSSIANS
● σ = 0.35 E^0.05
x σ = 0.35 LOG E − 0.05
▲ σ = 1.105/√E
γ MEAS
γ TRUE
3.0
2.8
2.6
2.4
2.2
2.0

Fig. 8

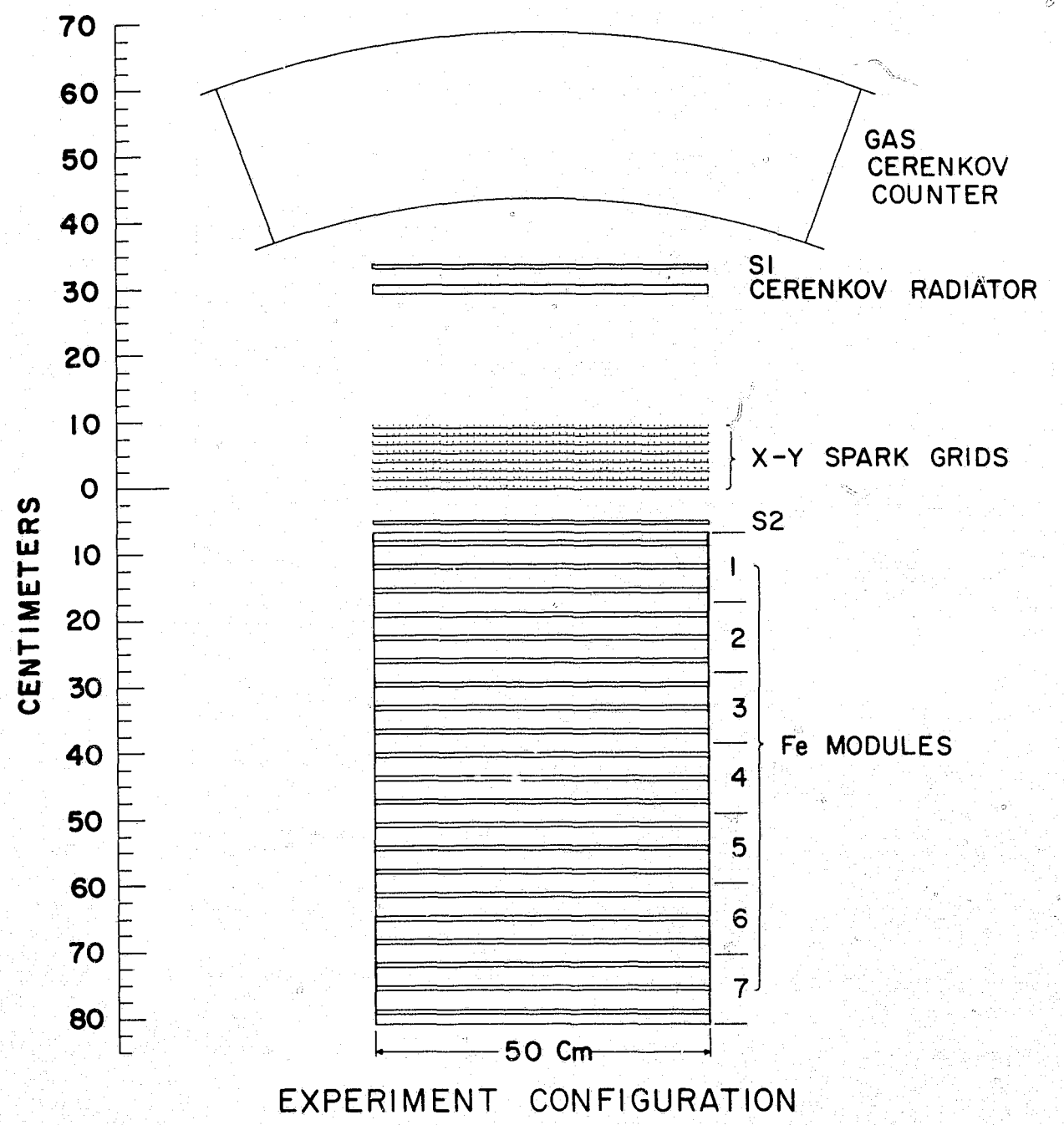

EXPERIMENT CONFIGURATION

Fig. 9

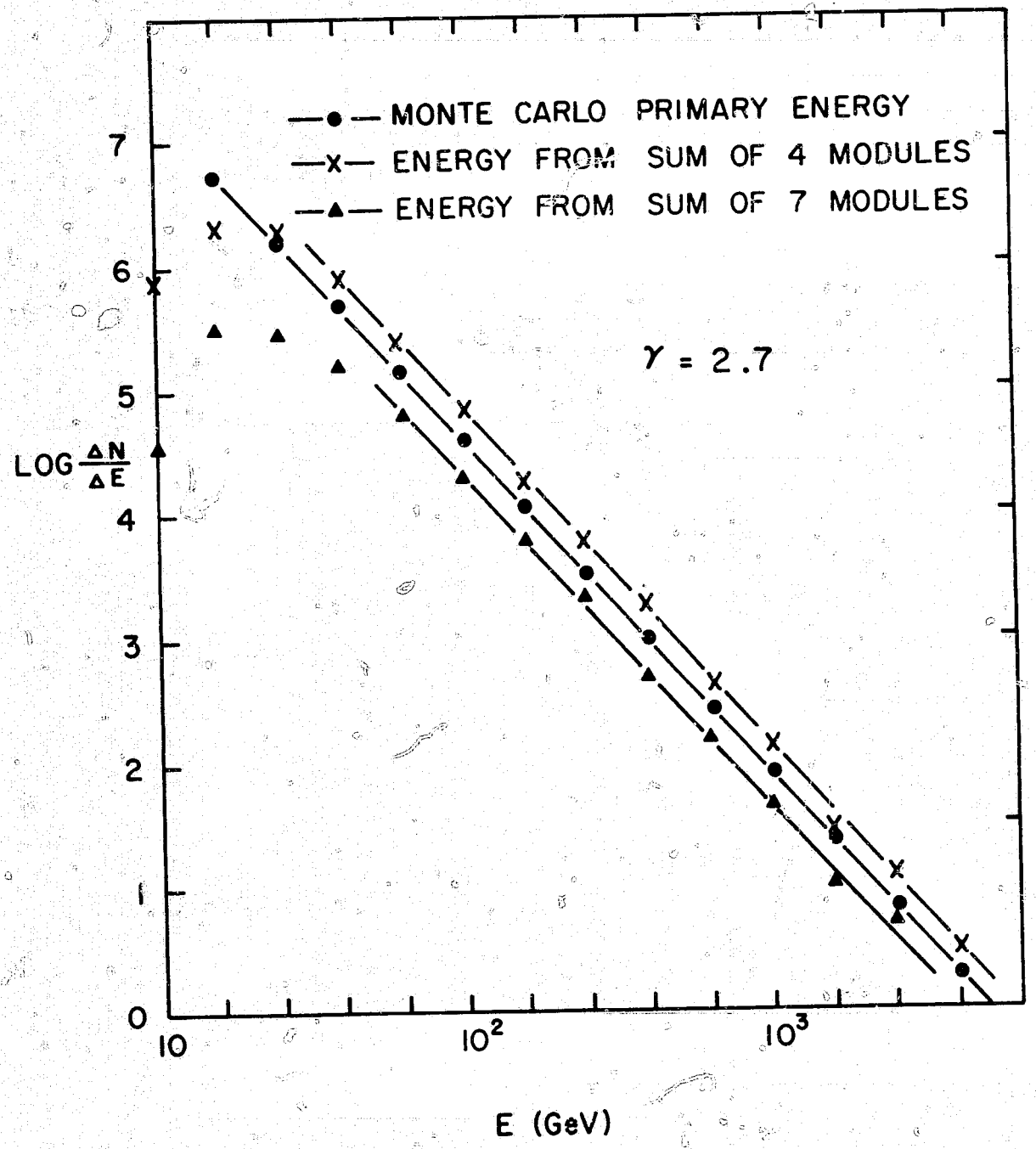
—●— MONTE CARLO PRIMARY ENERGY
—x— ENERGY FROM SUM OF 4 MODULES
—▲— ENERGY FROM SUM OF 7 MODULES
γ = 2.7
LOG ΔN/ΔE
E (GeV)
0
1
2
3
4
5
6
7
10
10²
10³

Fig. 10

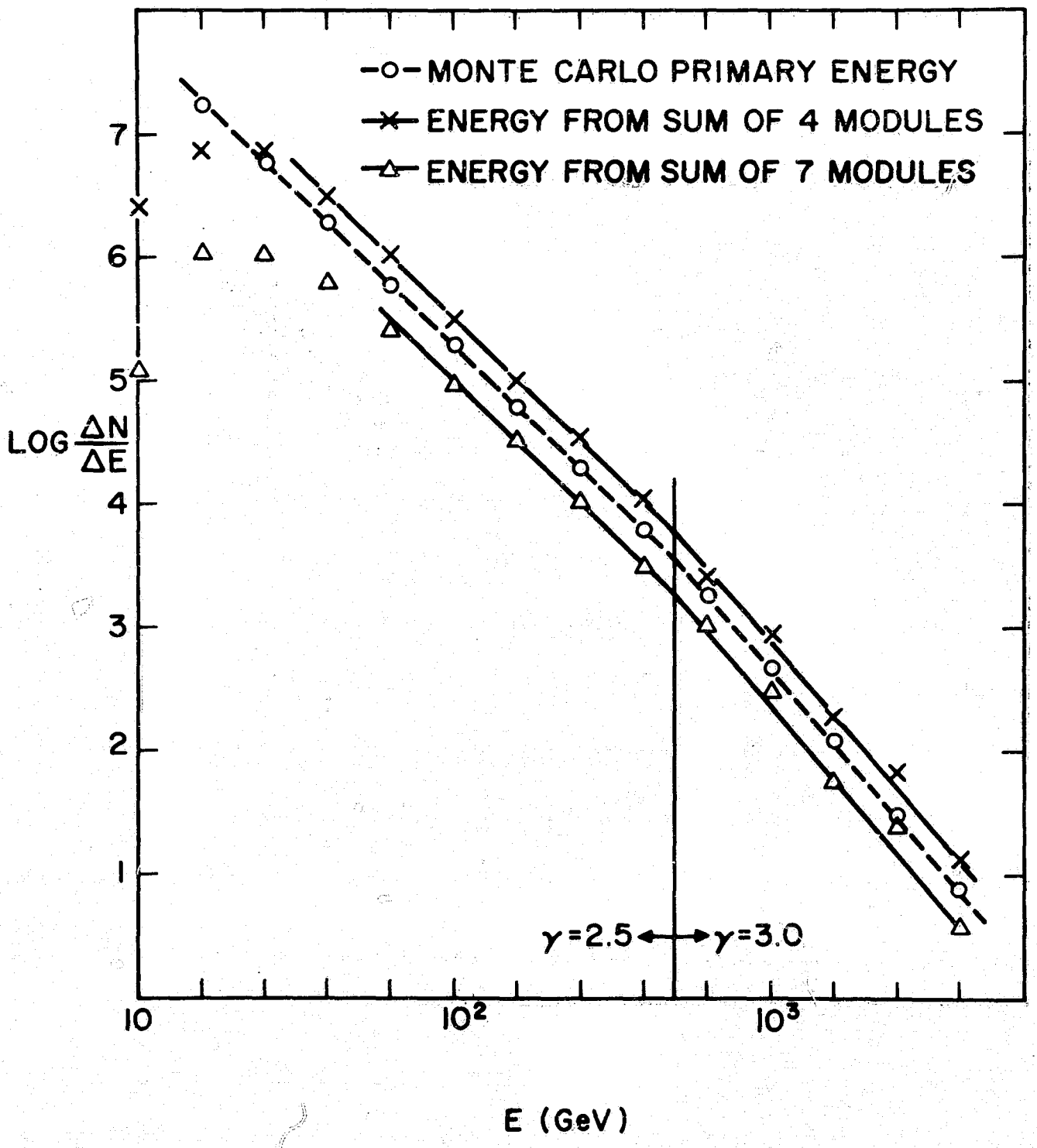
MONTE CARLO PRIMARY ENERGY
ENERGY FROM SUM OF 4 MODULES
ENERGY FROM SUM OF 7 MODULES
LOG ΔN/ΔE
7
6
5
4
3
2
1
γ=2.5
γ=3.0
10
10²
10³
E (GeV)

Fig. 11

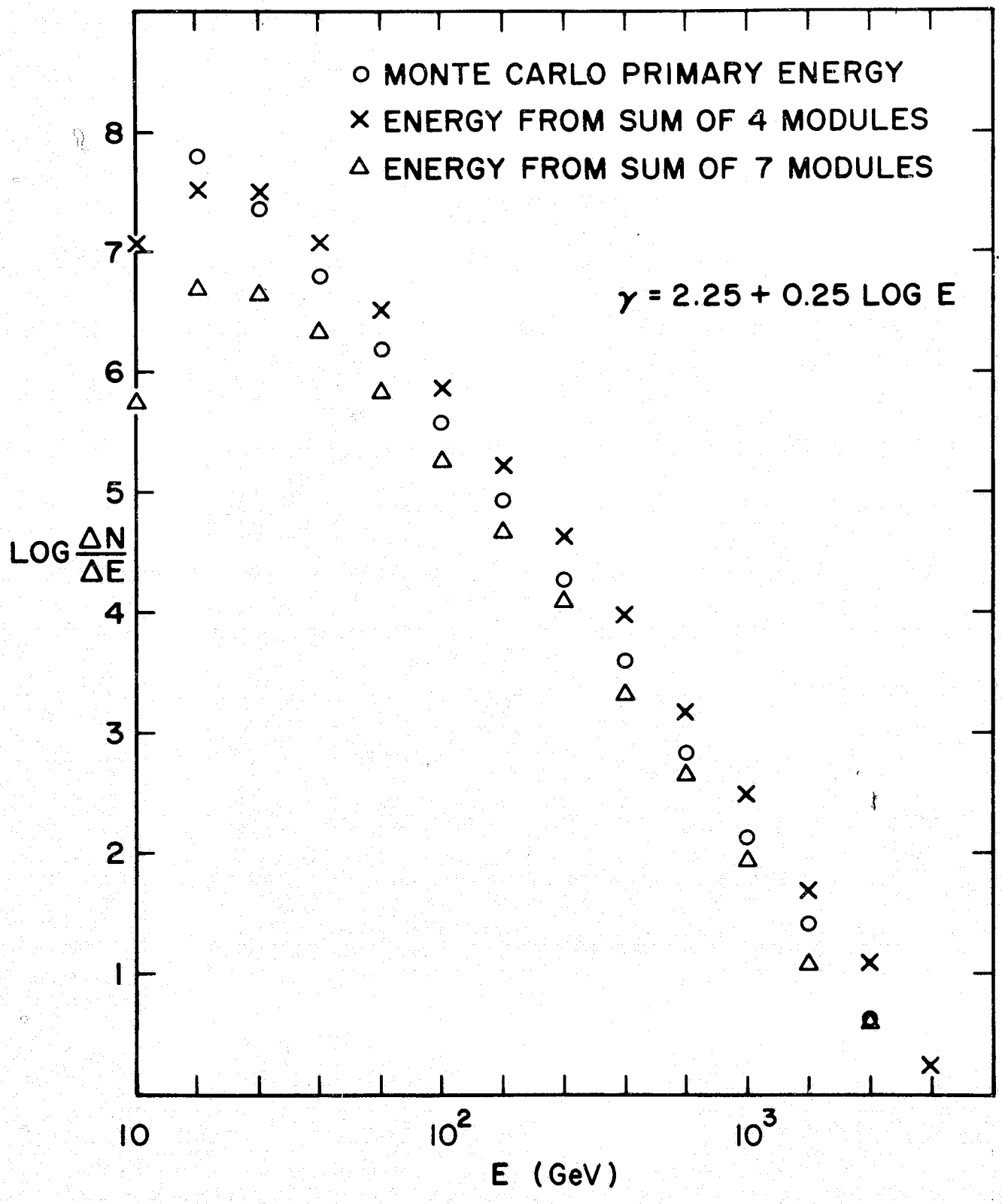
o MONTE CARLO PRIMARY ENERGY
× ENERGY FROM SUM OF 4 MODULES
Δ ENERGY FROM SUM OF 7 MODULES
γ = 2.25 + 0.25 LOG E
LOG ΔN/ΔE
8
7
6
5
4
3
2
1
10
10^2
10^3
E (GeV)

Fig. 12